Milestone 1.2.16. Reconciling the Impacts of Thermal Pretreatment on Radiation-Induced H_2 Generation from Aluminum-Clad Spent Nuclear Fuel Surrogate Materials

[INL/RPT-24-80453]
[Revision 0]

Technical Basis for Extended Dry Storage of Aluminum-clad Spent Nuclear Fuel

AUGUST 2024

Hanna Hlushko, Corey D. Pilgrim, Jacy K. Conrad, and Gregory P. Holmbeck

Center for Radiation Chemistry Research, Idaho National Laboratory

Elizabeth H. Parker-Quaife

Analytical Research Laboratory, Idaho National Laboratory

Joseph R. Wilbanks

Analytical Chemistry, Idaho National Laboratory

Idaho National Laboratory

Battelle Energy Alliance manages INL for the U.S. Department of Energy's Office of Nuclear Energy

[INL/RPT-24-80453]
[Revision 0]

Milestone 1.2.16. Reconciling the Impacts of Thermal Pretreatment on Radiation-Induced H_2 Generation from Aluminum-Clad Spent Nuclear Fuel Surrogate Materials

Hanna Hlushko, Corey D. Pilgrim, Jacy K. Conrad,
and Gregory P. Holmbeck
Center for Radiation Chemistry Research, Idaho National Laboratory

Elizabeth H. Parker-Quaife
Analytical Research Laboratory, Idaho National Laboratory

Joseph R. Wilbanks
Analytical Chemistry, Idaho National Laboratory

August 2024

Idaho National Laboratory
Center for Radiation Chemistry Research
Idaho Falls, Idaho 83415

http://www.inl.gov

Prepared for the
U.S. Department of Energy
Office of Environmental Management
Under DOE Idaho Operations Office
Contract DE-AC07-05ID14517

Page intentionally left blank

ABSTRACT, SUMMARY, FOREWORD, AND ACKNOWLEDGMENTS

To support the technical basis for the extended dry storage of aluminum-clad spent nuclear fuel (ASNF), thermal pretreatment procedures to minimize the radiation-induced generation of molecular hydrogen (H_2) have been investigated. The aim of thermal pretreatment is to eliminate the residual adsorbed water content on the ASNF's corrosion layers, precursors for H_2 generation. To date, irradiation studies in this area have found conflicting results for the effectiveness of thermal pretreatment procedures. The aim of this study was to reconcile those differences. However, the presented results, which utilized a modified *in situ* thermal pretreatment procedure, afforded H_2 yield data that further indicates that thermal pretreatment does not significantly reduce the radiation-induced yield of H_2 from gamma irradiated ASNF surrogate materials. Assessment of the differences between thermal pretreatment studies suggests that stainless-steel—present in the irradiation setup of studies that demonstrated a reduction in the yield of H_2 with thermal pretreatment—may afford not only unanticipated interfacial chemistry, but also the formation and radiolytic contribution of iron oxides to the chemistry underpinning the formation of H_2 in these systems. Given the Department of Energy Standard Canister—proposed for the extended dry storage of ASNF—is predominantly composed of stainless-steel, the potential contribution of stainless-steel and its corrosion layers to radiolytic H_2 production should be further investigated.

This research was funded by the U.S. Department of Environmental Management, Office of Technology Development, under contract DE-AC07-05ID14517.

Page intentionally left blank

CONTENTS

ABSTRACT, SUMMARY, FOREWORD, AND ACKNOWLEDGMENTS v
ACRONYMS x
1. INTRODUCTION 12
2. EXPERIMENTAL METHODS 13
2.1. Materials 13
2.2. Sample Preparation 14
2.3. Gamma Irradiations 15
2.4. Gas Phase Analysis 16
3. RESULTS AND DISCUSSION 16
4. CONCLUSIONS 19
5. ACKNOWLEDGMENTS 19
6. REFERENCES 20

FIGURES

Figure 1. Comparison of H2 yields (μmol kg^{-1}) as a function of absorbed gamma dose from the irradiation of pre-corroded aluminum alloy 6061 (AA6061) coupons in helium (He) environments with ~0% added relative humidity (RH): ambient-temperature-corroded vacuum drying only (●, INL)[27]; ambient temperature corroded vacuum drying + 4 hrs at 100 °C (■, INL) [27]; ambient temperature corroded vacuum drying + 4 hrs at 220 °C heating (▲, INL) [27]; high temperature corroded and air dried (▼, INL) [26]; "As-Corroded" Mini Canister (□, SRNL) [29]; "As-Corroded No Vacuum" Mini Canister (▽, SRNL) [33]; "150 °C As-Dried" Mini Canister (○, SRNL) [32]; and "220 °C As-Dried" Mini Canister (△, SRNL) [29]...13

Figure 2. Typical examples of flame-sealed, pre-corroded AA6061-T6 plate coupon samples before **(bottom)** and after **(top)** irradiation...14

Figure 3. (A) Complete modified Schlenk line heating cell assembly. **(B)** View of the heating tape with the thermocouple inserted between the ampule and heating tape...14

Figure 4. (A) Control sample setup highlighting the thermocouple feed through and ampule/coupon attachment. **(B)** Zoomed in image of the spotwelded control sample coupon...14

Figure 5. Calibration curve for the conversion of H2 peak area response into volume measured...16

Figure 6. Average concentrations of H2 (μmol kg^{-1}) as a function of absorbed cobalt-60 gamma dose from the irradiation of corroded AA6061-T6 plate coupons in He environments with ~0% added RH dried under vacuum with: (A) no thermal pretreatment (○ = this work, ● = previous INL study [27], and ⊙ = SRNL [33]); (B) 100–150 °C thermal pretreatment (□ = this work, ■ = previous INL study [27], and ⊡ = SRNL [33]); (C) 220 °C thermal pretreatment (▲ = this work, △ = previous INL study [27], and ◬ = SRNL [33]);

and (D) all data combined for comparison, with additional AA6061 samples that were not vacuum-dried or heated (▼ = previous INL study [26] and ▽ = SRNL [33])...17

TABLES

Table 1. Summary of pre-corroded AA6061-T6 plate coupon samples prepared for cobalt-60 gamma dose accumulation irradiations...15

Page intentionally left blank

ACRONYMS

AA6061	aluminum alloy 6061
ASNF	aluminum-clad spent nuclear fuel
DOE	United States Department of Energy
INL	Idaho National Laboratory
RH	relative humidity
SEM	Scanning electron microscope
SRNL	Savannah River National Laboratory
XPD	X-ray Powder Diffraction

Page intentionally left blank

Milestone 1.2.16. Reconciling the Impacts of Thermal Pretreatment on Radiation-Induced H_2 Generation from Aluminum-Clad Spent Nuclear Fuel Surrogate Materials

1. INTRODUCTION

The U.S. Department of Energy (DOE) currently manages an extensive inventory (~19,000 fuel assemblies) of aluminum-clad spent nuclear fuel (ASNF) [1, 2]. These assemblies are presently in interim storage, and are projected to be transferred into dry storage canisters for an extended period of time (> 50 years) pending final disposition [2-4]. During their lifetime, these fuel assemblies have been subjected to a combination of thermal and radiation-driven corrosion processes, resulting in the growth of compositionally complex corrosion layers, composed of aluminum oxides, hydroxides, and oxyhydroxides. These corrosion layers accommodate a large reservoir of adsorbed water and the elemental components to form molecular hydrogen (H_2), e.g., the hydroxyl groups (···OH) of (oxy)hydroxide mineral phases. In the presence of ionizing radiation fields, such as those arising from the contents of ASNF, these hydrated corrosion layers breakdown to yield H_2, which can diffuse into the surrounding environment [5-8]:

$$Al\cdots OH \rightsquigarrow h^+ + Al\cdots OH^-, \quad (1)$$

$$Al\cdots OH^- \rightarrow Al\cdots O^{\bullet -} + H^\bullet, \quad (2)$$

$$Al\cdots OH_2 + h^+ \rightarrow Al\cdots OH^- + H_{aq}^+, \quad (3)$$

$$H^\bullet + Al\cdots OH_2 \rightarrow H_2 + Al\cdots OH^\bullet, \quad (4)$$

$$H^\bullet + Al\cdots OH \rightarrow H_2 + Al\cdots O^\bullet, \quad (5)$$

$$H^\bullet + H^\bullet \rightarrow H_2. \quad (6)$$

Note, the oxygen component of these radiation-induced processes is retained within the corrosion layers [9]. The radiolytic generation of H_2 from ASNF is problematic for extended dry storage. Although initial concerns focused on hazards associated with the formation of explosive and flammable gas mixtures [10], the absence of radiation-induced oxygen production averts these scenarios [9, 10]. However, the accumulation of H_2 is still a concern as it may cause changes to material integrity, such as alloy embrittlement, and may pose safety concerns, such as pressurization of the DOE Standard Canister [3, 4, 11-17]. Consequently, the impacts of irradiation on ASNF systems is being investigated [18-33] as part of a DOE Office of Environmental Management-Technology Development program to evaluate the technical basis for the extended dry storage of ASNF [2].

A current focus of these investigations is the radiolytic implications of a thermal pretreatment of ASNF prior to sealing in a DOE Standard Canister [31]. The aim of thermal pretreatment is to eliminate the residual adsorbed water content of the ASNF's corrosion layers, thereby minimizing the radiation-induced generation of H_2. However, the formation of additional H_2 precursors and escape pathways as a result of heating has been reported in several publications, where aluminum oxyhydroxide powders have been irradiated after thermal pretreatment [34-39]. To date, gamma irradiation studies performed at Savannah River National Laboratory (SRNL)—using stainless-steel mini canisters—demonstrated that thermal pretreatment consistently affords significantly lower yields of H_2, irrespective of the irradiated aluminum sample's provenance, as shown in **Figure 1** [29, 32]. Similar studies performed at Idaho National Laboratory (INL)—involving pre-corroded aluminum coupons flame-sealed in borosilicate glass ampules—concluded that thermal pretreatment did not yield any significant difference in the total yield of H_2 within the investigated dose range, also shown in **Figure 1** [26, 27]. These differences in the impact of

thermal pretreatment on radiolytic H_2 generation may be attributed to differing sample preparation (*in situ* vs. *ex situ*) or irradiation methodologies (stainless-steel mini canisters *vs.* borosilicate glass ampules) between the two labs. At SRNL, thermal pretreatment of the corroded aluminum samples was performed *in situ* in the stainless-steel mini canisters they were ultimately irradiated in. Whereas at INL, the thermal pretreatment stage was performed *ex situ* in a vacuum oven, prior to removing and then flame-sealing in borosilicate glass ampules connected to a Schlenk line under slight vacuum.

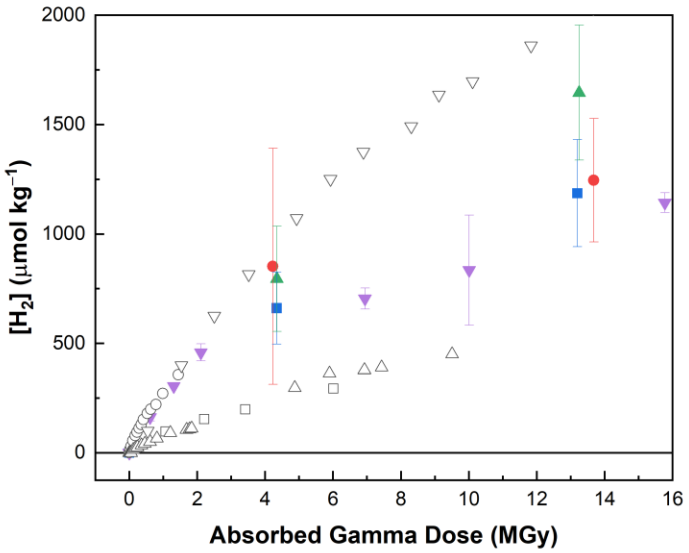

Figure 1. Comparison of H_2 yields (μmol kg^{-1}) as a function of absorbed gamma dose from the irradiation of pre-corroded aluminum alloy 6061 (AA6061) coupons in helium (He) environments with ~0% added relative humidity (RH): ambient-temperature-corroded vacuum drying only (●, INL)[27]; ambient temperature corroded vacuum drying + 4 hrs at 100 °C (■, INL) [27]; ambient temperature corroded vacuum drying + 4 hrs at 220 °C heating (▲, INL) [27]; high temperature corroded and air dried (▼, INL) [26]; "As-Corroded" Mini Canister (□, SRNL) [29]; "As-Corroded No Vacuum" Mini Canister (▽, SRNL) [33]; "150 °C As-Dried" Mini Canister (○, SRNL) [32]; and "220 °C As-Dried" Mini Canister (△, SRNL) [29].

Reconciling the divergence of these two conclusions is essential for determining the effectiveness of a thermal pretreatment process for minimizing radiolytic H_2 generation from ASNF under anticipated extended dry storage conditions. Here we report our findings from the use of a modified thermal pretreatment approach that provides *in situ* drying of pre-corroded AA6061 coupons in borosilicate glass ampules prior to flame-sealing and then irradiating with cobalt-60 gamma rays. The resulting H_2 yields provide systematic deconvolution of the factors impacting the differences in thermal pretreatment findings between INL and SRNL.

2. EXPERIMENTAL METHODS

2.1. Materials

This study used a previously sourced (QLab Corporation, Westlake, OH, U.S.) AA6061-T6 plate (8.00 cm × 30.48 cm × 0.13 cm, with six ¼ in. diameter holes for mounting) that had been cleaned, ambient-temperature-corroded (~350 days), dried, and sectioned (~0.61 cm × 2.57 cm × 0.13 cm individual coupons with an average mass of 0.53 g), the details for which can be found in reference [27]. Acetone (HPLC Plus, ≥ 99.9%), ethanol (absolute, ≥ 99.8%), iron(III) sulfate heptahydrate ($FeSO_4.7H_2O$, ≥ 99 %), sodium chloride (NaCl, 99.999 % trace metals basis), and sulfuric acid (H_2SO_4, 99.999 %) were supplied by MilliporeSigma (Burlington, Massachusetts, U.S.). Helium (He) was purchased in its highest available

purity from Norco Inc. (Boise, ID, U.S.). Ultra-pure water (18.2 MΩ·cm) was generated in-house using a ThermoScientific (Waltham, MA, U.S.) Harvey™ DI+ Cartridge System, and used for all water applications. Unless otherwise stated, all materials were used as received.

2.2. Sample Preparation

Samples comprised of a single AA6061-T6 plate coupon flame-sealed in a borosilicate glass ampule with ~0% added RH (as determined by an Omega HX200 series humidity sensor) He atmosphere, an example of which is shown in **Figure 2**. Prior to this, the glass ampules were preheated in a vacuum oven (VWR, Thermo Scientific oven model 6290) at 180 °C for a minimum of four hours to remove any residual water. The treated ampules were then left under vacuum at ambient temperature—overnight at a minimum—prior to installing on our bespoke Schlenk line for loading.

Figure 2. Typical examples of flame-sealed, pre-corroded AA6061-T6 plate coupon samples before **(bottom)** and after **(top)** irradiation.

To avoid re-adsorption of water following an AA6061-T6 plate coupon's thermal pre-treatment prior to flame-sealing, several modifications were made to our Schlenk line to enable thermal pre-treatment to be performed *in situ*. Firstly, the section of Schlenk line adjacent to the loaded borosilicate glass ampule was wrapped in heating tape (Brisk Heat BW0 high temperature insulated heating tape), as shown in **Figure 3A**. This section was heated 80 °C to facilitate additional moisture removal—using heating tape. Next, the ampule itself was fully wrapped with heating tape and then insulating tape (**Figure 3A**). A K-type thermocouple, connected to a temperature controller (Cole Palmer Digi-sense), was placed between the ampule and the heating tape to monitor the temperature throughout sample preparation (**Figure 3B**). This assembly was then secured in an outer boiling tube wrapped with an insulating blanket to minimize deviations in the temperature of the ampule's contents, as shown in **Figure 3A**.

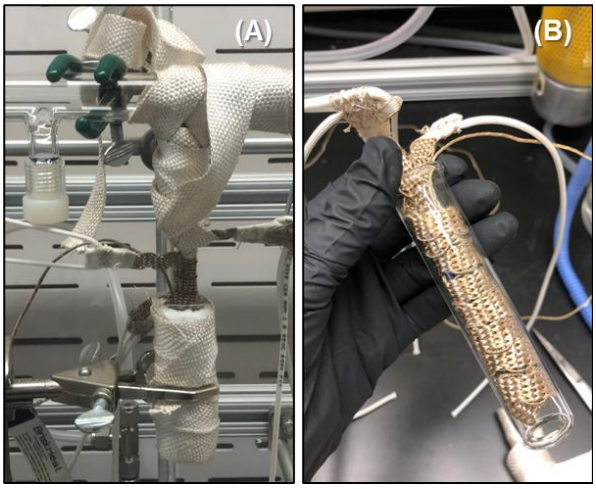

Figure 3. (A) Complete modified Schlenk line heating cell assembly. **(B)** View of the heating tape with the thermocouple inserted between the ampule and heating tape.

To evaluate this new setup prior to sample preparation, a control sample was engineered. A thermocouple was fed into an ampule through an adjacent port in the Schlenk line (**Figure 4**), split, and then affixed to the inside of the ampule (epoxy glue) and to an AA6061-T6 plate coupon (spotwelding). This approach enabled us to fine-tune our setup to ensure the correct temperature gradients were achieved and maintained for the duration of actual sample preparation.

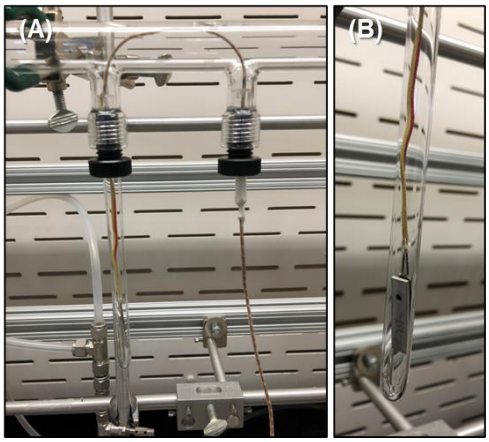

Figure 4. **(A)** Control sample setup highlighting the thermocouple feed through and ampule/coupon attachment. **(B)** Zoomed in image of the spotwelded control sample coupon.

For the preparation of a typical thermal pretreatment sample, a single AA6061-T6 plate coupon was loaded into a heat/vacuum-treated glass ampule and connected to the Schlenk line. Once interfaced, the line and loaded ampule were pump-purged three times with ~0% added RH He and house-vacuum (~5 × 10^{-3} Torr, as measured by a Kurt Lesker KJLC® Pirani

Gauge sensor). The system was then filled with ~0% added RH He and isolated. Under these conditions, the sample ampule was then heated to either 150 or 220 °C, corresponding to a temperature controller setpoint of 158 and 238 °C, respectively. Once the desired temperature was reached, the system was left to heat for one hour prior to opening to vacuum, refilling with He, and then opening to vacuum again. Following this thermal-vacuum treatment cycle, the system was allowed to cool under vacuum to ambient temperature (~24 °C) over one hour. After cooling, the system was subjected to one more He/vacuum cycle, after which it was backfilled with He at a slight vacuum (p = 0.84 bar) and flame-sealed.

2.3. Gamma Irradiations

Gamma dose accumulation irradiations were performed using the INL Center for Radiation Chemistry Research Foss Therapy Services (Pacoima, California, USA) Model 812 cobalt-60 gamma irradiator. Flame-sealed, pre-corroded AA6061-T6 plate coupon ampules were bundled into groups of three, with each bundle filling a specific position in the irradiator. Dose rates for each occupied irradiator position were established by chemical dosimetry using Fricke solution (1 mM $FeSO_4.7H_2O$ and 1 mM NaCl in 0.4 M H_2SO_4) [40] and a co-located Agilent (Santa Clara, CA, USA) Cary-60 UV-vis spectrophotometer. The calculated dose rates (67–411 Gy min^{-1}) were subsequently corrected for the radioactive decay of cobalt-60 ($\tau_{1/2}$ = 5.27 years, $E_{\gamma 1}$ = 1.17 MeV and $E_{\gamma 2}$ =1.33 MeV) and aluminum metal electron density vs. water (0.8673) [20, 25, 41]. Samples were irradiated under ambient irradiator temperature (~40 °C) conditions for a given amount of time to attain accumulated gamma doses of approximately 2.5, 5.0, 15, and 45 MGy as per Fricke dosimetry. Control samples accounted for 0 MGy of received gamma dose. A summary of this study's irradiated samples is given in **Table 1**.

Table 1. Summary of pre-corroded AA6061-T6 plate coupon samples prepared for cobalt-60 gamma dose accumulation irradiations.

Sample set	**Thermal pretreatment**	**Ampule #**	**Coupon mass** (g)	**Accumulated Dose** (MGy)
1	None	61	0.53553	39.2
		62	0.47494	
		64	0.44979	
2	None	63	0.52912	13.8
		65	0.53934	
		66	0.52226	
3	None	72	0.56511	4.5
		73	0.53723	
		74	0.54279	
4	None	75	0.53018	2.2
		76	0.52711	
		77	0.54419	
5	150 °C	81	0.55182	38.9
		82	0.54912	
		83	0.54123	
6	150 °C	84	0.55075	13.0
		85	0.54616	
		86	0.53377	
7	150 °C	87	0.54211	4.4
		88	0.52192	
		89	0.51396	
8	150 °C	90	0.53480	2.2
		91	0.52164	

		92	0.56534	
9	220 °C	68	0.56133	38.9
		69	0.55569	
		70	0.54046	
10	220 °C	78	0.55075	13.3
		79	0.51983	
		80	0.54244	
11	220 °C	94	0.54472	4.4
		95	0.55574	
		96	0.51968	
12	220 °C	97	0.55044	2.2
		98	0.55112	
		99	0.44367	

Note: Control samples with no coupon present were also irradiated for each thermal pre-treatment.

2.4. Gas Phase Analysis

Post irradiation, sample ampules were recovered, and their contents analyzed for H_2 by gas chromatography using a Shimadzu Co. (Kyoto, Japan) Nexus GC-2030 gas chromatograph equipped with a dielectric-barrier discharge ionization detector. As with our previous studies, a crush-tube approach was used, the methodology and instrument settings for which have been previously described [20, 25]. This approach was slightly modified here by backfilling the crush tube with 10 psi of ultra-high purity helium (He, NorLAB, Boise, ID, U.S.) prior to cracking the ampule. Calibration curves for this study were prepared by injecting known quantities of H_2 from calibration gas sources—1 vol% H_2 in He (Airgas, Idaho Falls, ID, U.S.) either used directly or diluted to 0.2 vol% H_2 in He in a Tedlar bag with a calibrated 500 mL syringe. Results from these calibrations are shown in **Figure 5**, from which an average instrument response, in terms of peak area per mole of H_2, was determined to be $1.694 \times 10^{12}\,mol^{-1}$. Quality control checks were performed daily to confirm known concentrations of H_2 relative to measured calibration curves.

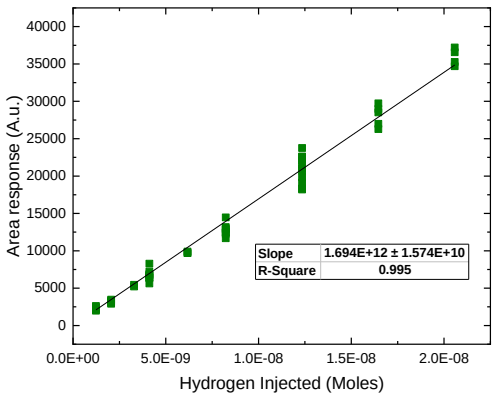

Figure 5. Calibration curve for the conversion of H_2 peak area response into volume measured.

3. RESULTS AND DISCUSSION

The gamma radiation-induced formation of H_2 from the three systems targeted by this study are shown in **Figure 6**. Plotted alongside this work are the previous data reported by INL and SRNL for the thermal pre-treatment of corroded aluminum materials [26-29]. Note, a small discrepancy was found in the processing of the H_2 measurements in reference [27]. The headspace volumes used for the derivation of

some H_2 amounts were incorrect and have now been amended using an ampule average of 3.40 ± 0.07 mL. Although these corrections have a negligible effect on the previous report's findings, the amended data are presented below in **Figure 6**, cited to the original report [27].

Our new findings, using the aforementioned alternative thermal pretreatment procedure, are consistent with our previous data—the yield of H_2 increases with increasing absorbed gamma dose, and shows little dependence on thermal pretreatment procedure.

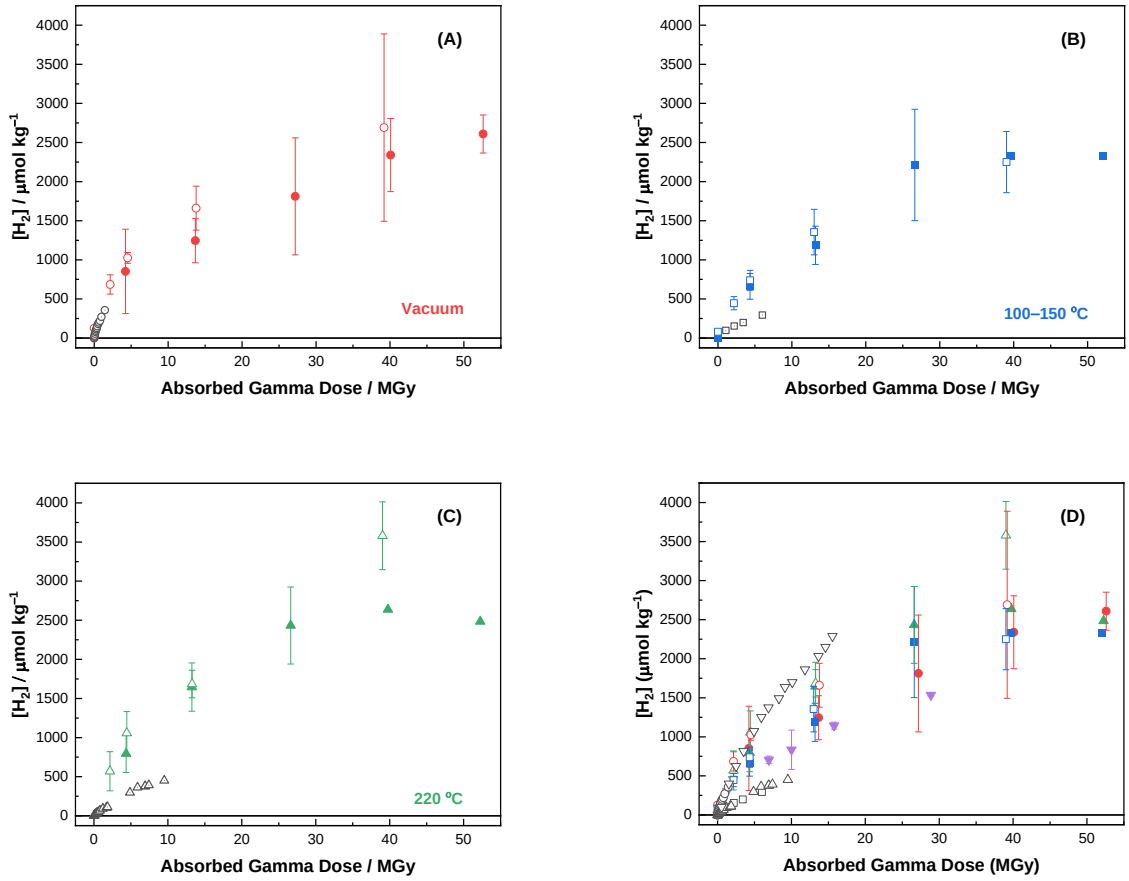

Figure 6. Average concentrations of H_2 (µmol kg^{-1}) as a function of absorbed cobalt-60 gamma dose from the irradiation of corroded AA6061-T6 plate coupons in He environments with ~0% added RH dried under vacuum with: **(A)** no thermal pretreatment (○ = this work, ● = previous INL study [27], and ⊙ = SRNL [33]); **(B)** 100–150 °C thermal pretreatment (□ = this work, ■ = previous INL study [27], and ⊡ = SRNL [33]); **(C)** 220 °C thermal pretreatment (▲ = this work, △ = previous INL study [27], and ◬ = SRNL [33]); and **(D)** all data combined for comparison, with additional AA6061 samples that were not vacuum-dried or heated (▼ = previous INL study [26] and ▽ = SRNL [33]).

The internal consistency of both the INL and SRNL thermal pretreatment data suggests that the *ex situ* vs. *in situ* mode by which the thermal pretreatment process was performed is not the root cause of the conflicting conclusions. Although differences in sample preparation may be responsible, we can confirm that under the conditions of our alternative thermal pretreatment procedure: (i) no H_2 was detected from irradiated controls (i.e., in the absence of a coupon), and thus, there was no significant amount of residual moisture in our glass ampoules post thermal pretreatment; (ii) humidity was not reintroduced by our Schlenk line's He backfill source, again, because of the absence of H_2 above background measurements in our treated controls, but also because we have historically shown that elevated RH increases the yield of H_2 from irradiated pre-corroded and pristine aluminum coupons [20, 42]; and (iii) there is no evidence of

organic contamination—the irradiation of which would provide an additional source of H_2—as no carbon-based radiolysis products (e.g., carbon dioxide, CO_2, and methane, CH_4) were detected, despite our gas chromatography method having the capacity to measure these potential species. With these observations in mind, the source of the H_2 yield discrepancy between the INL and SRNL thermal pretreatment studies is not obvious, especially given that many factors influence the radiation-induced formation of H_2 from our surrogate ASNF systems.

A potential explanation may be found in the types of aluminum samples used, given that the SRNL and INL experiments varied in terms of size, surface area, and corrosion layer composition—the latter due to differences in pre-corrosion procedure and thermal pretreatment atmospheres. The INL studies used a long-term, ambient-temperature corroded AA6061-T6 plate (8.0 cm × 30.5 cm × 0.13 cm, exposed for 350 days in ambient temperature water), which was freshly cut into coupons (~0.61 cm × 2.57 cm × 0.13 cm), potentially exposing fresh aluminum metal or, more likely, aluminum oxide to our radiation environments. However, potential concerns surrounding whether the presence of aluminum metal/aluminum oxide would inflate our H_2 yields—thereby masking any thermal pretreatment effect—can be dismissed here as the INL data are in good agreement with a previous INL study that utilized AA6061 coupons that did not exhibit exposed aluminum metal/aluminum oxide [24, 26]. Scanning electron microscopy (SEM) showed an average corrosion layer thickness of 8 ± 3 μm, although some areas exceeded 15 μm [43]. SEM imaging also showed that thermal pretreatment with vacuum and heating caused a change in oxide morphology prior to irradiation, with the 220 °C samples exhibiting deep cracks. The INL AA6061-T6 plate coupon corrosion layers were also characterized via X-ray diffraction (XRD), and found to be predominantly composed of bayerite, with no significant contribution from other oxyhydroxide phases. Note, drying at 220 °C showed a loss of any peaks associated with the corrosion layer, probably due to the sample cracks exposing the underlying bulk aluminum metal/aluminum oxide interface. The cracks could also potentially provide additional surface area for H_2 precursors and for H_2 to adsorb [43]. The surface area of aluminum oxide and (oxy)hydroxides has been shown previously to have an effect on radiolytic H_2 production in these systems [37-39, 44].

The SRNL studies used an assembly of 17 individual, 0.13 cm thick, AA6061-T6 plates, bolted together and corroded at ambient temperature for only 33–41 days. Surface characterization on the plate segments showed a similar corrosion layer thickness of 5–10 μm, primarily made of bayerite in all samples. The SRNL studies also saw cracks forming in the samples that underwent thermal pretreatment to 220 °C. Their 220 °C thermal pretreatment procedure afforded a reduction in the bayerite XRD pattern intensity, and an increase in the prominence of boehmite, indicating partial conversion of the hydroxide to oxyhydroxide. The conversion of the bayerite to boehmite was not seen in the INL studies, perhaps because the thermal pretreatment was performed under vacuum or He atmosphere (INL), as opposed to in air (SRNL). Given the larger contribution of boehmite in the SRNL corrosion layers following a 220 °C thermal pretreatment, an elevated yield of H_2 would have been expected upon irradiation, as based on the findings of aluminum oxide/(oxy)hydroxide powder studies [34-39]. For example, for a 200 °C thermal pretreatment, increased H_2 yields were observed and attributed to an increased contribution of boehmite/pseudo boehmite to the radiation response of the system [38]. This was not the case in the SRNL mini canister studies, and both dried samples showed a similar reduction in the H_2 yield, despite the fact that bayerite conversion to boehmite is not expected at 150 °C, suggesting that another factor may be at work. Unfortunately, the SRNL studies did not characterize the plates heated to 150 °C to confirm that no additional boehmite was formed.

A clear distinction between the INL and SRNL studies is the sample vessel employed. The INL samples were flame-sealed in He backfilled borosilicate glass ampules under slight vacuum (p ~ 12 psi), while the SRNL assemblies were sealed in stainless-steel mini canisters pressurized with He (p ~ 24 psi). This difference in containment materials may provide an explanation for the observed thermal pretreatment discrepancies. Where the INL samples have been thermally pretreated both *in situ* and *ex situ*, and then irradiated, the SRNL assemblies have only been thermally pretreated *in situ* within the stainless-steel mini canister they were ultimately irradiated in. This is an important observation, as stainless-steel and its

corrosion products (iron oxides) are known to influence the yield of H_2 from water radiolysis [45-47]. With this in mind, an argument could be made for the interaction of a thermally pretreated stainless-steel surface—as in the case of the SRNL studies—with the various radiolytic mechanisms and behaviors benchmarked by our previous studies. This postulation could be evaluated by performing an *ex situ* thermal pretreatment prior to sealing an aluminum assembly in a mini canister for irradiation, or by backfilling a thermally pretreated cannister with humid air for irradiation.

A final factor to consider is differences in H_2 sampling techniques. The INL borosilicate glass ampules are "single-shot" analyses performed after they have attained a specified absorbed dose. This approach ensures that the headspace pressure is consistent throughout, and that residual H_2 production processes post irradiation are complete, giving a total H_2 yield. For the SRNL mini canister experiments, H_2 measurements are made by sampling the headspace of the same vessel multiple times over the duration of the irradiation. As such, the reported H_2 yields are cumulative values at the time of sampling, i.e., adding the yield of H_2 measured at that specific sampling time to that measured at a previous time. A concern with repeat measurements from the same vessel is the impact of changes in the headspace pressure and gas composition on radiolytic H_2 production.

Overall, it is still unclear as to why the INL and SRNL thermal pretreatment studies afforded contradictory H_2 results. Although there are many differences between the two studies—for which Occam's razor may indicate that the reason for the thermal pretreatment discrepancy is because they are so different to begin with—we postulate that the stainless-steel comprising the SRNL mini-canisters is a non-innocent bystander that, once thermally pretreated, may provide additional chemical pathways for the system's radiolysis product to interact with, thereby influencing the radiolytic production of H_2.

4. CONCLUSIONS

The aim of this study was to reconcile conflicting findings on the impacts of thermal pretreatment on the radiation-induced generation of H_2 from ANSF surrogate materials in support of the technical basis for extended dry storage of ASNF [27, 28, 33]. The presented results, which utilized a modified *in situ* thermal pretreatment procedure, afforded H_2 yield data that confirmed our original findings, that is thermal pretreatment does not significantly reduce the radiation-induced yield of H_2 from gamma irradiated AA6061-T6 plate coupons under the investigated conditions. Assessment of the differences between the two laboratories approaches to these thermal pretreatment experiments suggest that the stainless-steel comprising the SRNL mini-canisters is a non-innocent bystander [28-33]. We propose that the *in situ* thermal cycling and radiation exposure of the stainless-steel surfaces may afford not only unanticipated interfacial chemistry, but also the formation and radiolytic contribution of iron oxides to the chemistry underpinning the formation of H_2 in these systems.

Given the DOE Standard Canister is predominantly composed of stainless-steel, the potential contribution of stainless-steel and its corrosion layers to radiolytic H_2 production should be investigated. To address this technical knowledge gap, we propose a further comparative study between irradiations of identical aluminum coupons closed in stainless-steel vessels and borosilicate ampules that have been subject to a thermal pretreatment. Each container type would be sealed with a He atmosphere with a range of added RH (~0, ~50, and ~100%), and then gamma irradiated. The irradiated atmospheres would then be analyzed for H_2, and the stainless-steel vessel subject to surface characterization.

5. ACKNOWLEDGMENTS

This research was funded by the U.S. Department of Environmental Management, Office of Technology Development, under contract DE-AC07-05ID14517.

6. REFERENCES

1. Energy, D.o., *Spent Fuel Database (SFD), Version 8.0.7*. 2021.
2. Eidelpes, E., et al., *Technical basis for extended dry storage of aluminum-clad spent nuclear fuel.* Journal of Nuclear Materials, 2023. **577**: p. 154299.
3. Argyle, M.D., *Aluminum Clad Spent Nuclear Fuel: Technical Considerations and Challenges for Extended (>50 Years) Dry Storage, DOE/ID RPT 1575*. 2017.
4. Jarrell, J.J. and M.J. Connolly, *Aluminum Clad Spent Nuclear Fuel Long Term Dry Storage Technical Issues Action Plan - Technical and Engineering Activities*. 2017: United Kingdom.
5. Buxton, G.V., et al., *Critical Review of rate constants for reactions of hydrated electrons, hydrogen atoms and hydroxyl radicals JÅOH/Åq in Aqueous Solution.* Journal of Physical and Chemical Reference Data, 1988. **17**: p. 513-886.
6. Milosavljevic, B. and J. K Thomas, *Reactions of Electrons on the Surface of ??-Al2O3. A Pulse Radiolytic Study with 0.4 MeV Electrons.* The Journal of Physical Chemistry B, 2003. **107**.
7. Thomas, J.K., *Physical Aspects of Radiation-Induced Processes on SiO2, γ-Al2O3, Zeolites, and Clays.* Chemical Reviews, 2005. **105**(5): p. 1683-1734.
8. Le Caër, S., *Water Radiolysis: Influence of Oxide Surfaces on H2 Production under Ionizing Radiation.* Water, 2011. **3**(1): p. 235-253.
9. Conrad, J.K. and G.P. Horne, *Milestone 1.2.12: The Fate of Oxygen Radical Species in Corroded Aluminum Alloys under Irradiation*. 2023: United States. p. Medium: ED; Size: 13 p.
10. d'Entremont, A.L., *Oxygen Limit for Flammability of a Gas Mixture of Helium – Hydrogen – Oxygen in the U.S. Department of Energy Standard Canister Storage Demonstration.* 2024.
11. Department of Energy, *Preliminary design specification for Department of Energy standardized spent nuclear fuel canisters. Volume 1: Design specification*. 1998: United States.
12. Department of Energy, *Preliminary design specification for Department of Energy standardized spent nuclear fuel canisters Volume 2: Rationale document*. 1998: United States. p. 46.
13. Snow, S., *ECAR 4632, Supplemental Evaluation of the DOE Standard SNF Canister for Accidental Drops*. 2019.
14. Ambat, R. and E.S. Dwarakadasa, *Effect of hydrogen in aluminium and aluminium alloys: A review.* Bulletin of Materials Science, 1996. **19**(1): p. 103-114.
15. Gangloff, R.P. and B.P. Somerday, *Gaseous Hydrogen Embrittlement of Materials in Energy Technologies: The Problem, its Characterisation and Effects on Particular Alloy Classes*. 2012: Elsevier Science.
16. Lu, G. and E. Kaxiras, *Hydrogen embrittlement of aluminum: the crucial role of vacancies.* Physical review letters, 2005. **94**(15): p. 155501.
17. Bonin, B., M. Colin, and A. Dutfoy, *Pressure building during the early stages of gas production in a radioactive waste repository.* Journal of Nuclear Materials, 2000. **281**: p. 1-14.
18. Parker-Quaife, E.H., et al., *Radiation-Induced Molecular Hydrogen Gas Generation by Pre-Corroded Aluminum Alloy 1100*. 2019.
19. Parker-Quaife, E.H., et al., *Radiation-Induced Changes in Corrosion of AA1100*. 2019.
20. Parker-Quaife, E.H., et al., *Radiation-induced molecular hydrogen gas generation in the presence of aluminum alloy 1100.* Radiation Physics and Chemistry, 2020. **177**: p. 109117.
21. Horne, G.P., et al., *Complete Round-Robin Hydrogen Gas Analysis Capability Comparison (Milestone 2.6)*. 2020: United States.
22. Parker-Quaife, E.H. and G.P. Horne, *Milestone 2.8: Preliminary Radiolytic Gas Generation Measurements from Helium-Backfilled Samples*. 2020: United States.
23. Horne, G.P. and E.H. Parker-Quaife, *Milestone 2.7: Evaluation of Techniques for the Measurement of Molecular Hydrogen Gas in Helium Matrices*. 2020: United States.
24. Horne, G.P., et al., *Milestone 1.2.9: Radiolytic Gas Generation Measurements from Helium Backfilled Samples of AA1100 and AA6061 Coupons*. 2021: United States.

25. Conrad, J.K., et al., *Radiolytic Gas Production from Aluminum Coupons (Alloy 1100 and 6061) in Helium Environments—Assessing the Extended Storage of Aluminum Clad Spent Nuclear Fuel.* Materials, 2022. **15**(20): p. 7317.
26. Horne, G.P., et al., *Milestone 1.2.10: Steady-state H_2 "roll over" point data for aluminum alloys 1100 and 6061*. 2022: United States.
27. Pilgrim, C.D., et al., *Milestone 1.2.11: H_2 Production from Surrogate "Non-Native" Corrosion Plumes on Aluminum 6061-T6 Fuel Cladding Surrogates*. 2022: United States.
28. Verst, C.G. and A.L. d'Entremont, *Measurement of radiolytic hydrogen generation and impact of drying treatments on reactor exposed and surrogate aluminum materials*. 2021: United States.
29. Verst, C., et al., *Interim Irradiation and Measurement of As-Dried vs As-Corroded Hydrated Oxide Specimens (Large Coupons)*. 2021.
30. d'Entremont, A.L., et al., *Radiolysis testing of SNF materials and surrogates in a "Mini-Canister"*, in *Conference: Waste Management Symposia 2022 Phoenix, AZ March 6-10, 2022*. 2022: United States.
31. d'Entremont, A.L., *ASNF Drying Recipe - Review Data*. Savannah River National Laboratory.
32. Verst, C., *Mini-canister radiolysis results – Preliminary results of alternate drying recipe* 2022.
33. Verst, C. and A.L. d'Entremont, *Final mini-canister results summary*. 2024: United States.
34. Huestis, P., et al., *Radiolytic stability of gibbsite and boehmite with adsorbed water.* Journal of Nuclear Materials, 2018. **501**: p. 224-233.
35. LaVerne, J.A. and P.L. Huestis, *H Atom Production and Reaction in the Gamma Radiolysis of Thermally Modified Boehmite.* The Journal of Physical Chemistry C, 2019. **123**(34): p. 21005-21010.
36. Kaddissy, J.A., et al., *Efficient Hydrogen Production from Irradiated Aluminum Hydroxides.* International Journal of Hydrogen Energy, 2019. **44**(7): p. 3737-3743.
37. Kaddissy, J., et al., *Radiolytic Events in Nanostructured Aluminum Hydroxides.* The Journal of Physical Chemistry C, 2017. **121**.
38. Briley, E., et al., *Radiolysis of thermally dehydrated gibbsite.* Materials Chemistry and Physics, 2021. **271**: p. 124885.
39. Shen, Z., et al., *Diffusion Mechanisms of Radiolytic Species in Irradiated Al (Oxy-)Hydroxides.* The Journal of Physical Chemistry C, 2018. **122**(50): p. 28990-28997.
40. Fricke, H., *The Oxidation of Fe to Fe by the Irradiation with X-Rays of Solutions of Ferrous Sulfate in Sulfuric Acid.* Journal of chemical physics., 1935. **3**(1): p. 60-61.
41. Spinks, J.W.T. and R.J. Woods, *An Introduction to Radiation Chemistry*. 3 ed. 1990, United States of America: John Wiley & Sons. 504.
42. Kesterson, R.K., et al., *Evaluation of Radiolysis Data for Hydrogen Gas Generation During Gamma Irradiation of Pre-Corroded and Pristine Aluminum Samples - An Aluminum SNF Dry Storage Study Interim Report*. 2020: United States. p. Medium: ED; Size: 24 p.
43. Holmbeck, G.P., et al., *Milestone 1.2.14: Surface Characterization of Irradiated Surrogate Non-Native Corrosion Plumes on Aluminum 6061-T6 Specimens*. 2023: United States.
44. Redaoui, D., et al., *Mechanism and Kinetic Parameters of the Thermal Decomposition of Gibbsite Al(OH)3 by Thermogravimetric Analysis.* Acta Physica Polonica: A, 2017. **131**(3): p. 562-565.
45. McGrady, J., et al., *H_2 generation at metal oxide particle surfaces under γ-radiation in water.* Journal of Nuclear Science and Technology, 2020. **58**(5): p. 604-609.
46. Ali, I., et al., *Hydrogen production and stainless steel corrosion during water decomposition under gamma radiation.* Radiation Physics and Chemistry, 2024. **223**: p. 111902.
47. Yoshida, T., et al., *Enhanced Gamma-Ray Energy Conversion in Water Vessels—Part II: Hydrogen Production by Water Radiolysis.* Nuclear Science and Engineering, 2005. **150**(3): p. 357-361.